Quantifying and Understanding Structural Loading from Wave-Driven Debris Fields

Dakota Mascarenas[1]*, Michael R. Motley, Ph.D., P.E.[1], Marc O. Eberhard Ph.D.[1], Pedro Arduino, Ph.D.[1], Abbey Serrone[1]

[1]Department of Civil & Environmental Engineering, University of Washington, Seattle, WA 98107, USA

**correspondence to:* Dakota Mascarenas (dakotamm@uw.edu)

ABSTRACT

During a tsunami or storm surge event, coastal infrastructure and ports are subject to a series of disparate physical hazards that can cause significant damage and loss of life. Among these, debris impact loading during inundation events is chaotic, complex, and thus far minimally understood, especially when considering the accumulation of individual debris into a large debris field. This work provides the results of a comprehensive experimental study of the impact and subsequent damming of chaotic debris fields, including more than 400 individual trials; this scope of this paper describes the experimental design and initial analysis of wave-driven debris-induced loading for select configurations. These data include both the impact phenomena and subsequent damming by debris accumulation and finds strong correlation between increasing debris field density and high impact forces. High frequency impact forces and low frequency damming signals are considered via Fast Fourier Transform methods. Overall trends in wave-induced debris forcing from large debris fields are presented.

INTRODUCTION

Inundation events, such as tsunamis and storm surges, pose a significant threat to coastal communities and infrastructure globally. Damage within these communities is not only caused by flowing water, but also by debris from collapsed structures, vegetation, and whatever might be moved by an inundation flow. Previous studies have investigated wave- and flow-induced debris loading. For example, Ko et al. (2015) and Naito et al. (2016) experimentally studied tsunami-propelled shipping container impacts, but focused on single debris impact. Studies of larger debris fields have tended to focus on accumulation and transport in lieu of impact and damming. Yao et al. (2014) focused on solitary wave-driven debris. Schmocker and Hager (2011) investigated accumulations of debris at river bridges, which was observed to be highly chaotic in nature. Naito et al. (2014) posed a procedure to evaluate potential for debris impact in specific area.

Despite an impressive body of work, there are few studies that investigate the impact and damming forces caused by debris fields (i.e. multiple pieces of debris) carried by inundation-type flows. The impacts from dense debris fields are chaotic in nature and it can be difficult to predict how the disparate debris will interact with a coastal structure. This can be especially relevant inside of ports which tend to consist of a significant number of potential pieces of large-scale debris within an area of complex flow. While single-debris impacts are fairly predictable and reproducible, debris fields require a statistically-driven approach.

To gain understanding of structural loading induced by large-scale, flow-driven debris fields, this study presents the preliminary results of a comprehensive experimental program in the Large Wave Flume at the NHERI Wave Research Lab in order to generate a statistically-representative data set of various multi-debris scenarios and provide measurements to inform numerical modeling efforts. While the essentially non-deterministic aspects of the underlying phenomena present a challenge, this study employs high volume testing and analysis.

Tsunami-like inundation was simulated by pushing water via piston-driven wavemaker over a simulated bathymetry and toward an instrumented test structure. The structure was subjected to the run-up wave and follow-on flow. Idealized debris fields in the form of up to (32) rectangular, high-density polyethylene (HDPE) blocks were introduced to the flow via a removable frame, by which an initial condition was set. The testing protocol created many different test configurations in order to create a broad sweep of initial conditions by varying the following: (i) number of debris, (ii) debris field configuration, (iii), debris field density, (iv) frame type (either static surface condition or condition as randomized via dropping from a magnetized frame approximately 3.3 ft (1 m) above the water surface), and (v) wave type (i.e. unbroken or bore-like on contact with the test structure). A total of (41) tests were conducted with (10) trials each. The large volume of data is intended to shed light on the non-deterministic phenomena underlying flow-driven debris fields.

The test structure was instrumented with load cells in three-dimensions and pressure sensors. Acoustic doppler velocimeters (ADVs) and wave gauges (both wire and ultrasonic) were used to capture flow characteristics. Hi-speed camera and GoPro footage was captured for every test. Additionally, several debris were outfitted using multiaxial accelerometers, which were remotely controlled for each trial.

Long term, this study will systematically analyze data collected during the large-scale testing program and present the following advances in understanding: (i) interactions between a debris-field, fluid, and stationary structure; (ii) comparison between a single debris tests and large-scale debris field; (iii) trends in three-dimensional structural loading from a debris field as correlated with initial condition; and (iv) rigid body dynamics of a flow-driven debris field. The results presented here represent an initial, broad examination of the general trends found during the test program. A more comprehensive discussion of these tests is presented by Mascarenas (2022).

EXPERIMENTAL DESIGN

Testing was performed over a 10-week period at the NHERI O.H. Hinsdale Wave Research Laboratory at Oregon State University in Corvallis, OR. The test was conducted in the Large Wave Flume, which is approximately 340 ft (104 m) long, 12 ft (3.7 m) wide, and 15 ft (4.6 m) tall. A piston-driven wave maker capable of simulating tsunami-like and swell waves is situated at the south end, capable of driving a variety of wave profiles in water up to 6.6 ft (2 m) deep for tsunami-like waves, and 8.9 ft (2.7 m) deep for swell-type waves. The coordinate system is defined $(x, y, z) = (0, 0, 0)$ at the bottom of the flume in the center of the front face of the wave maker paddle at its rest position. Positive x is in the streamwise direction of wave propagation, positive z is upward, and positive y is based on a right-hand coordinate system toward the flume wall.

For this experiment, concrete panels were laid to create simulated beach bathymetry and induce run-up. The bathymetry was laid out similarly to previous experiments such as Winter et al. (2020), Alam et al. (2020), and Shekhar et al. (2020). Figure 1 provides a plan and elevation view of the flume, sloped at 1:12 then increased to 1:24. Figure 1 shows flume elevation and plan views with bathymetry and test structure in place. Also shown is the location of the debris frame (discussed below), placed 6.6 ft (2 m) upstream of the test structure.

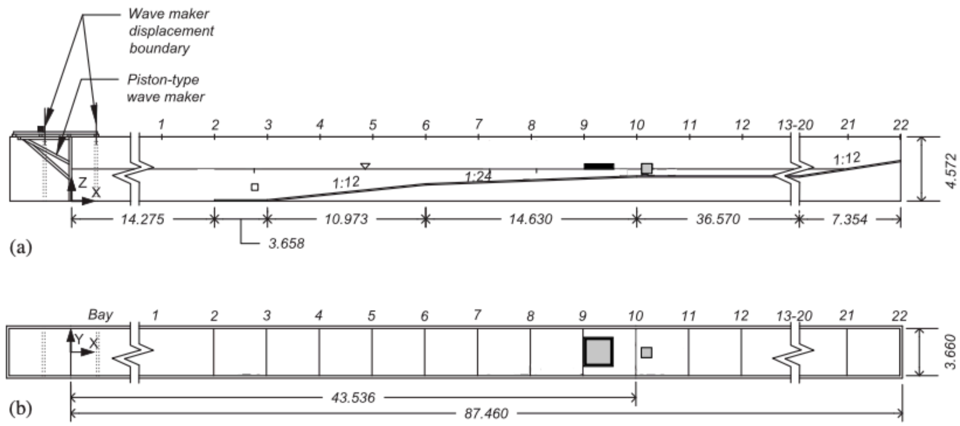

Figure 1. Flume and bathymetry elevation (top) and plan (bottom) in m (adapted from Winter et al. (2020)). Debris frame location is also shown.

A 40 in. (1.02 m) square base x 24 in. (0.61 m) tall box constructed with sheet metal and piped steel framing (similar to Alam et al. (2020)) was placed at approximately 144 ft (43.8) m from the face of the neutral wave maker and was subjected to run-up and follow-on flow. The structure was supported via low-friction bearings from a frame mounted to the flume wall sides, allowing degrees of freedom in the streamwise *x*, transverse *y*, and vertical *z* directions. (8) load cells were located at the points of attachment. Underneath the structure were 10 in. (0.25 m) steel "legs", which were not loadbearing but were installed to be just above the bathymetry beneath. Figure 2 shows the test structure in experimental position.

Figure 2. Test structure in flume.

Instrumentation included (8) load cells ((2) in-line streamwise, (2) in-line transverse, and (4) pancake load cells on the four top corners of the orange box to measure uplift), (11) pressure sensors in the front of the box, (7) acoustic doppler velocimeters, (3) wave gauges, and (6) ultrasonic wave gauges. Acoustic doppler velocimeters and pressure sensors were removed for trials with debris to prevent damage. All data discussed in this paper was sampled at 1200 Hz. Figure 3 shows load cell instrumentation on the test structure.

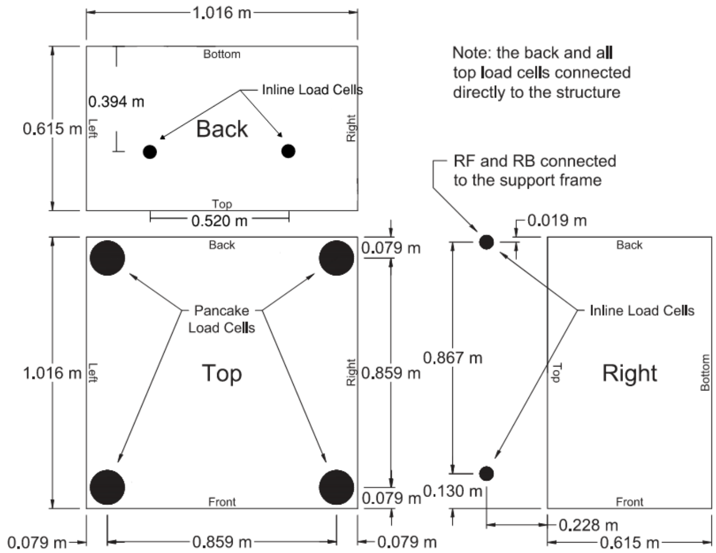

Figure 3. Location of load cells on test structure (adapted from Winter et al. 2020).

Debris fields were experimentally simulated using idealized debris pieces made of high-density polyethylene (HDPE). The debris were 20 in. (0.51 m) long and 2 in. (0.051 m) x 4 in. (0.102 m) in cross-sectoin and weighed approximately 5.56 lb (2.52 kg). Within this scope, a maximum of (24) full-sized pieces were used. The density of HDPE is 61.7 lb/ft^3 (988 kg/m^3) (i.e. approximately neutrally buoyant in fresh water) and the Young's modulus is 116 ksi (0.8 GPa). The draft of the debris was approximately 2 in. (5 cm).

Debris were outfitted with a compartment for onboard accelerometers. The construction required a hole at the geometric center of the HDPE block to allow for the accelerometer to be oriented specifically. In order to maintain neutral buoyancy and draft, portions of HDPE were selectively removed to maintain axial symmetry but reduce overall weight. While specific accelerometer data is outside of the scope of this work, modifications to the stiffness of the overall block are assumed negligible.

The debris field initial condition was static at the beginning of all tests in this scope and was manipulated between trials. To make initial conditions repeatable, a wooden frame was installed 6.6 ft (2 m) upstream from the face of the box to contain floating debris. The largest frame interior dimension was 6.6 ft x 6.6 ft (2 m x 2 m), although framing members extended throughout the width of the flume to provide rotational stability. The frame was outfitted with adjustable minor framing members to create initial field dimensions. The wooden frame floated freely on the water surface and was operated manually by an overhead crane to lift above the height of the wave before wave motion reached the debris field.

WAVE GENERATION

Waves were created using the O.H. Hinsdale Large Wave Flume wavemaker. The wavemaker is driven by pistons and has a 13.2 ft (4 m) stroke, with the coordinate system in the flume defined by the "resting" position at the center of the stroke extents.

For repeatability and consistency with earlier trials conducted as documented by Alam et al. (2020), the study conducted most testing using an unbroken, error function wave. The wave is highly symmetric and exhibits minimal turbulence, simulating inundation-like flow with a long wave period and remaining unbroken throughout the length of the testing area. The unbroken wave was an error function (*erf*) profile for piston movement (Winter et al. (2020)) with a still water level (SWL) of 6.6 ft (2 m) and an amplification of 500. The piston movement utilized nearly the full stroke of the paddle over approximately 10 seconds.

Wave gauge data shown in Figure 4 shows the wave profiles as recorded at a wave gauge approximately 23 ft (7 m) upstream of the structure. The datum is the SWL. The DAQ recording is around 200 seconds, with the primary wave signal passing at approximately 35 seconds.

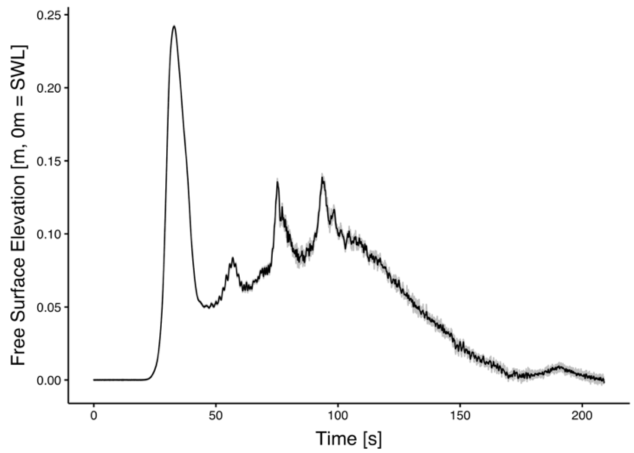

Figure 4. Free surface elevation during unbroken wave at wire wave gauge located approx. 23 ft (7 m) upstream of test structure. Grey lines represent (6) individual trials conducted (wave only, no debris). The black line is the trial-averaged free surface elevation per timestep.

Figure 4 also shows the consistency of the wave itself. (6) trials are represented in gray; black indicates the free surface elevation averaged between each trial for each timestep. Given minute variation, especially in the primary wave signal region between 30 and 45 seconds, we conclude that variation between trials subjected to this wave profile are due to debris impacts to both the structure and flow.

DEBRIS CONFIGURATIONS

Within the scope of this paper, (19) total tests are discussed. All initial debris fields were symmetric about the centerline of the flume in the streamwise direction. The debris fields within this scope were varied by the following:

1. **Configuration Type ("Regular" versus "Random"):** indicates whether the debris were tightly packed in a rectangular format or randomly arranged within a pre-described initial debris field size, effectively varying field surface area density.
2. **Number of Debris:** (1), (8), (16), and (24) full-sized only debris configurations were tested.
3. **Orientation/Debris Field Size:** within "Regular" configurations, indicates whether or not the debris were oriented in the with long axis in direction of flow (longitudinally, "L") or perpendicular to the direction of flow (transverse, "T"); within "Random" configurations, indicated the initial debris field bounds

Figure 5 shows the layouts discussed. (10) "regular" tests with (10) trials each and (9) "random" tests with (10) trials each were conducted for this scope.

The “regular” tests are categorized as individual pieces having either a longitudinal or transverse orientation to the direction of flow. For each number of debris tested, at least one longitudinal and transverse test was conducted. With (16) debris, (4) total tests were conducted and are labeled “L1”, “L2, “T1”, and “T2” in subsequent discussion. We consider the initial debris field density to be 100% with regular tests, as the debris are tightly packed. Since the face dimension of the test structure is only approximately (1) meter, it is possible for larger configurations to have individual debris pieces miss the structure without impact.

The “random” tests consist of different square dimensions within which the debris is initially placed filled with the allotted number of debris. By varying both the field maximum dimension (e.g., area in which the debris can spread out) and the number of debris, we are able to achieve a surface area density from approximately 20% to 80%. We can compare the “Regular” and “Random” tests using debris field density.

The top left diagram in Figure 5 (below) is labeled “1L”. For future discussion, the median peak impacts due to a single debris from all (10) trials oriented longitudinally on the center axis are taken to normalize median peak impacts from all other trials considered.

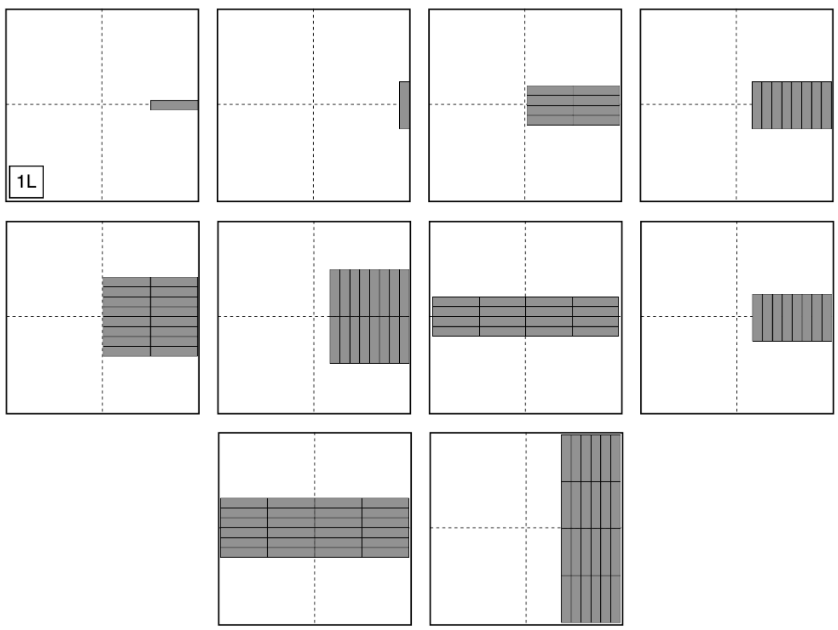

(a)

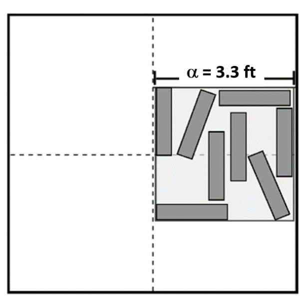

(b) *typ.*

Figure 5. (a) "Regular" configurations are tightly packed. (b) a typical “Random" configuration is shown ((8) pieces of debris in 1mx1m initial field extents). Flow direction is from left to right.

Figure 5(b) is typical of the (9) “random” configurations. In this case, (8) individual debris were placed within a 3.3 ft x 3.3 ft (1 m x 1 m) square by hand and with no specific position; we define α equal to the side dimension of the initial debris field square and can calculate an initial debris field density. Table 1 of the (9) “random” configurations is shown below. The table shows number of debris, debris initial field size, and initial field density for all (9) “random” tests. By varying the field dimension and number of debris and comparing with tightly-packed “regular” configurations, field density can become a predictor of structural impacts as discussed in the following section.

No. of Debris	α (ft)	Initial Field Density (debris area/field area)
8	2.5	0.73
8	3.3	0.41
16	3.3	0.82
16	4.1	0.52
16	4.9	0.36
24	4.1	0.78
24	4.9	0.54
24	6.6	0.31
24	6.6 x 12.1*	0.17

*Table 1. (9) "random" test configurations with number of debris, debris field density dimensions, and calculated initial field density. * indicates a non-square initial field: this configuration used the full flume as limiting width.*

STREAMWISE LOADING DURING UNBROKEN WAVE WITH DEBRIS

This section focuses on preliminary analysis of streamwise loading due to the symmetric nature of the flow and since primary impacts occur at the front (upstream) face of the structure. The summation of the two streamwise load cells placed at the same elevation (see Fig. 3) provides the loading transmitted via the test structure due to debris impact.

Wave Only

First, we measure the loading due to the wave without debris. Note: given that wave and debris loading phenomena occur primarily between 25 and 50 seconds, the sampling rate is reduced from 1200 Hz to 20 Hz outside of that time period in post-processing for this and following time histories. Figure 6 shows the total streamwise loading as recorded by (2) streamwise load cells (shown in Fig. 3). In the absence of debris, the wave loading is consistent between trials. Given the predictability of the wave profile shown in Figure 4, this is expected.

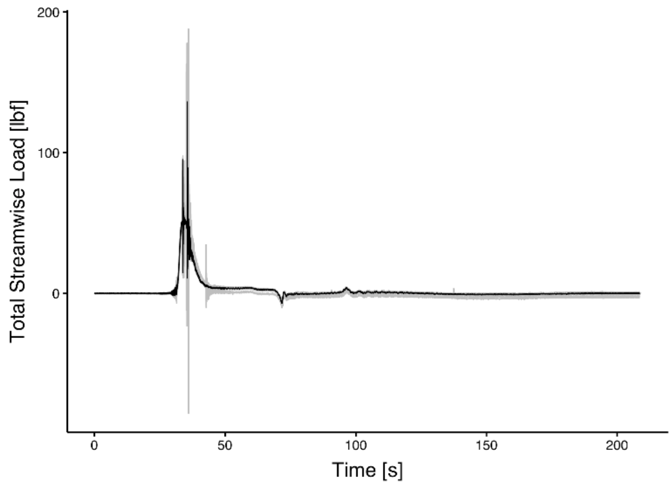

Figure 6. Total streamwise load time history due to wave only.

Single Debris Impacts

To understand the complexity of observed phenomena, first the impacts due to single debris were analyzed. Figure 7 shows (10) different trials conducted given a single, full-size piece of debris, oriented with its long axis in the direction of flow (labeled "1L": one debris oriented longitudinally) with the emphasized time history corresponding to the trial nearest to the *median* peak streamwise force across trials. While the DAQ recorded for more than 200 seconds, data around the wave impact (between 30 and 45 seconds) is shown below since it represents the most significant forcing events. For this preliminary analysis, peak forces for one experimental configuration are taken as the *median* peak of all trials.

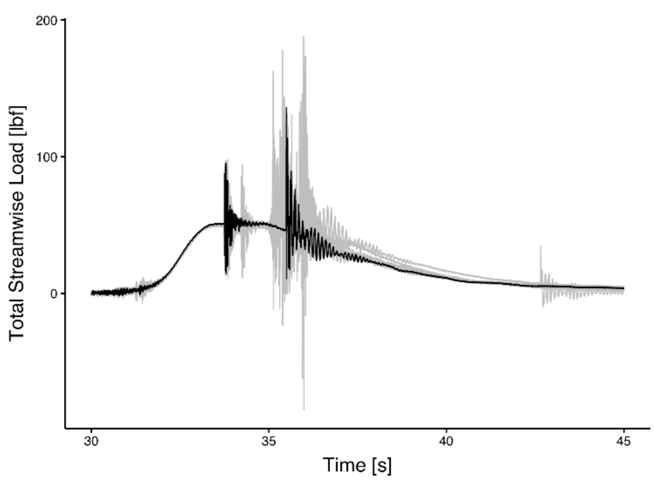

Figure 7. Total streamwise load time history due to (1) debris oriented longitudinally (1L).

Figure 7 above also shows two individual impact events: one occurring before approximately 34 seconds, and one occurring after 34 seconds. We observed that the two peaks are caused by (1) an initial impact of the leading face of the debris field and (2) chaotic interactions between debris and the structure as debris is forced around and under during the inundation event. This pattern is persistent in all trials presented.

Preliminary Spectral Analysis

Additionally, Figure 7 shows lower frequency loading persists which represents increased forcing due to wave forcing and debris damming. This is consistent with observations from Shekhar et al. (2020). Following the method shown in Shekhar et al. (2020) to perform a Fast Fourier Transform to debris impact signals then applying a high pass filter (filtering out below 4 Hz) and a low pass filter (filtering out above 4 Hz), one can observe the two impacts as well as potential damming and hydrodynamic forces. Figure 8 shows time histories reconstructed with an Inverse Fast Fourier Transform with both filters. We note that individual peak forces are maintained with the low pass filter applied; thus, impact forces are high frequency events.

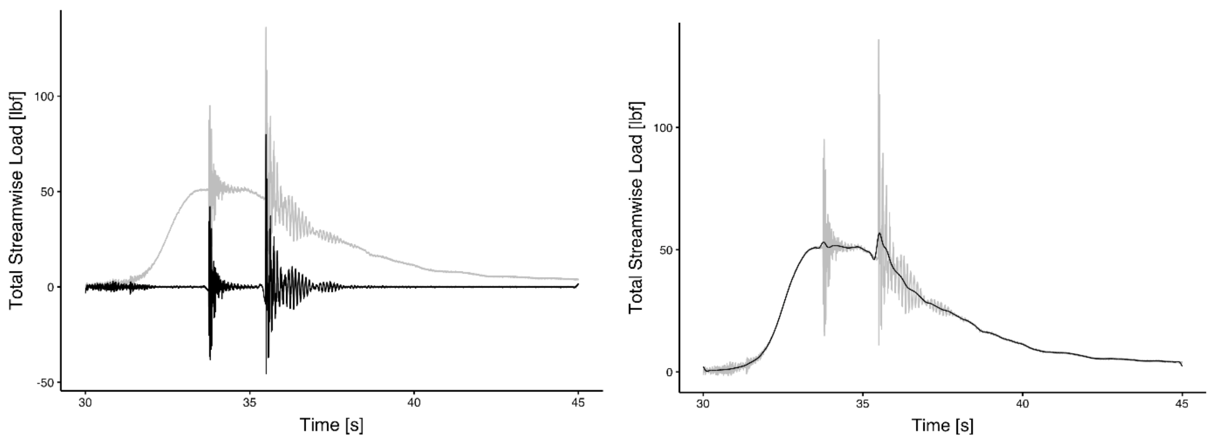

Figure 8. High pass filter (left) and low pass filter (right) applied to time history of 1L trial.

Figure 8 highlights the clear distinction between high and low frequency loading on the test structure in the streamwise direction. Low frequency forcing is due to hydrodynamic forcing (i.e. the wave), and also may show damming forces due to debris becoming caught and effectively increasing cross-sectional area after the initial impact. The single, longitudinal debris (1L) showed little damming potential, but another test conducted with (8) total debris oriented transverse to the direction of flow with higher damming potential is shown in Figure 9 with a low pass filter. Note that the trial shown is one of (10) conducted trials, with peak value nearest to the mean trial peak value.

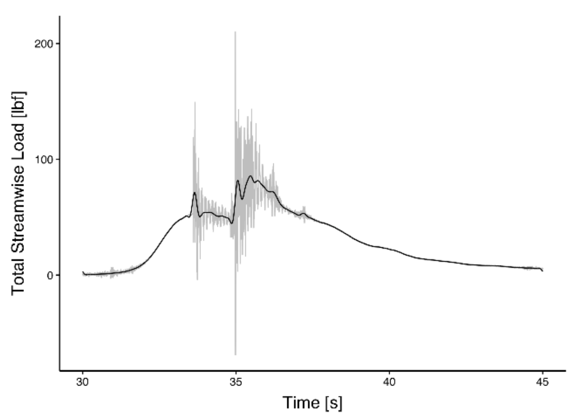

Figure 9. Low pass filter applied to total streamwise load time history for a "regular" trial with (8) debris with debris oriented transverse to the direction of flow.

Figure 9 shows a lingering forcing after the "second" impact and represents a significant load applied to the structure. This is the physical manifestation of increased surface area caused by debris damming which changes the effective area impacted by the flowing water. Because the hydrodynamic forcing on the structure is a direct function of the impacted area, this results in increased loading during wave inundation.

Median Peak Forces

We apply an effective measure of central tendency by taking each trial's peak force for all (19) "Regular" and "Random", then take the *median* value of between each test's (10) trials. Note: (6) of the 190 considered trials were omitted due to instrumentation error, with no less than (8) valid trials included for each test. Each test shows similar events as those observed with a single piece of debris: a first impact occurs before 34 seconds and a second impact occurs after 34 seconds. Normalizing by the reaction in the streamwise direction due to a longitudinally-oriented single debris (1L) during *each* event (i.e. both the first and second peaks), the following plots shown in Figure 10 indicate the median peak force across trials for all (19) tests, arranged according to initial debris field density.

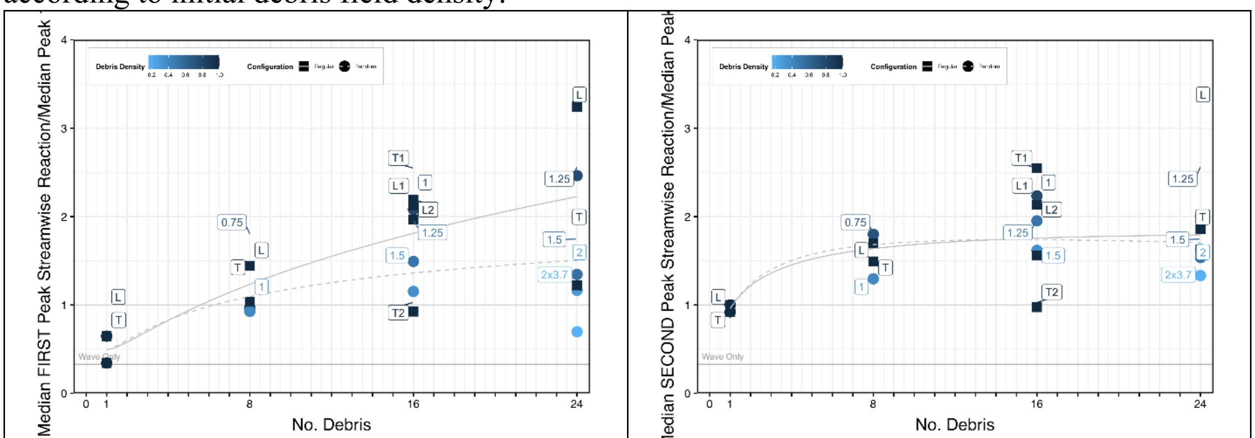

(a) first impact | (b) second impact

Figure 10. Median peak forces for (19) tests, varying by debris density and number of debris, and normalized. First impact is (a); second impact is (b).

The above results appear to show significant correlation during both the first and second impacts: a higher density debris field tends to yield higher median peak forces than lower density debris fields. We again note that "regular" debris fields with 100% initial field density are labeled "L" or "T" depending on the orientation direction of individual debris and "random" debris fields are indicated by their maximum extents in meters. Tests are grouped by the number of debris and colored by the initial debris field surface density.

We observe that for the same number of debris, more tightly packed debris fields have higher impacts. This is particularly apparent in the first impact. In general, we observe longitudinal ("L") configurations applying higher loading in the first impact. In particular during the second impact, there are instances where transverse ("T") configurations with many more debris have similar forces to even single debris tests, despite higher mass in the debris field. This is likely due to the fact that many debris may miss the structure. Additionally, the transverse configurations tend to move more slowly in the vicinity of the structure, resulting in reduced impact forces.

CONCLUSION

This study shows the initial findings of a multi-phase analysis of the trends in debris field interaction with a test structure in an experimental setting. The test structure and debris were subjected to inundation-like flow conditions of known hydrodynamic properties. The interaction of debris with each other and with a test structure is highly chaotic in nature. Trends in loading patterns and differences in loading between debris field initial conditions were identified: 1) within time histories, there are two discernable impact peaks in addition to post-impact damming forces; 2) increasing peak loads are strongly correlated with increasing initial debris field density.

This work represents the first presentation of the results from this set of experiments. Additional data post-processing is underway to expand these results, including but not limited to the effect of variability in the composition of the debris field on force measurements, examination of interactive impact forces between individual pieces of debris within a debris field, transverse and uplift force effects. This data is also valuable for future model validation and refinement and it is expected that this unique dataset will provide a starting point for a more comprehensive probabilistic study of various debris fields and their interaction with more complex coastal structures.

This becomes increasingly important for ports and similar coastal areas, as the complexity of the flows and nature of the debris within these facilities can be difficult to model experimentally at the scale required to predict loading. Tsunami and storm surge events inherently cause significant damage to coastal infrastructure, and port facilities are no exception. There is ongoing research exploring the movement of debris fields within these facilities, and this work serves to extend concepts in debris tracking and accumulation to provide designers with additional information to improve the resilience of port facilities worldwide.

ACKNOWLEDGEMENTS

This research was funded by the National Science Foundation's Natural Hazards Engineering & Resilience Institute (NHERI) via grant #203791. The team thanks the staff at O.H. Hinsdale Laboratory for their substantial contributions to the project.

REFERENCES

Alam, M. S., Winter, A. O., Galant, G., Shekhar, K., Barbosa, A., Motley, M., Eberhard, M., Cox, D., Arduino, P., and Lomonaco, P. (2020). "Tsunami-like wave induced lateral and uplift pressures and forces on an elevated coastal structure." Journal of Waterway, Port, Coastal, and Ocean Engineering, 146(4).

Ko, H. T.-S., Cox, D. T., Riggs, H. R., and Naito, C. J. (2015). "Hydraulic experiments on impact forces from tsunami-driven debris." Journal of Waterway, Port, Coastal, and Ocean Engineering, 141(3), 04014043.

Mascarenas, D.M., *Experimental Evaluation of Loads from Inundation-Driven Debris Fields*, MSCE Thesis, University of Washington, 2022.

Naito, C., Cercone, C., Riggs, H. R., and Cox, D. (2014). "Procedure for site assessment of the potential for tsunami debris impact." Journal of Waterway, Port, Coastal, and Ocean Engineering, 140(2), 223–232.

Naito, C., Riggs, H. R., Wei, Y., and Cercone, C. (2016). “Shipping-container impact assessment for tsunamis.” Journal of Waterway, Port, Coastal, and Ocean Engineering, 142(5), 428 05016003.

Schmocker, L. and Hager, W. H. (2011). “Probability of drift blockage at bridge decks.” Journal of Hydraulic Engineering, 137(4), 470–479.

Shekhar, K., Winter, A. O., Alam, M. S., Arduino, P., Miller, G. R., Motley, M. R., Eberhard, M.O., Barbosa, A. R., Lomonaco, P., Cox, D. T. (2020). Conceptual Evaluation of Tsunami Debris Field Damming and Impact Forces. Journal of Waterway, Port, Coastal, and Ocean Engineering,146(6), 04020039.

Winter, A. O., Alam, M. S., Shekhar, K., Motley, M., Eberhard, M., Barbosa, A., Lomonaco, P., Arduino, P., and Cox, D. (2020). “Tsunami-like wave forces on an elevated coastal structure: Effects of flow shielding and channeling.” Journal of Waterway, Port, Coastal, and Ocean Engineering, 146(4).

Yao, Y., Huang, Z., Lo, E. Y. M., and Shen, H.-T. (2014). “A preliminary laboratory study of motion of floating debris generated by solitary waves running up a beach.” Journal of Earthquake and Tsunami, 08(03), 1440006.